Development 133, 4655-4665 (2006) doi:10.1242/dev.02650

Bchs, a BEACH domain protein, antagonizes Rab11 in synapse morphogenesis and other developmental events

Rita Khodosh[1,2], Adela Augsburger[1], Thomas L. Schwarz[2] and Paul A. Garrity[1,3,*]

BEACH proteins, an evolutionarily conserved family characterized by the presence of a BEACH (Beige and Chédiak-Higashi) domain, have been implicated in membrane trafficking, but how they interact with the membrane trafficking machinery is unknown. Here we show that the *Drosophila* BEACH protein Bchs (Blue cheese) acts during development as an antagonist of Rab11, a small GTPase involved in vesicle trafficking. We find that reduction in, or loss of, *bchs* function restores viability and normal bristle development in animals with reduced *rab11* function, while reductions in *rab11* function exacerbate defects caused by *bchs* overexpression in the eye. Consistent with a role for Bchs in modulating Rab11-dependent trafficking, Bchs protein is associated with vesicles and extensively colocalized with Rab11 at the neuromuscular junction (NMJ). At the NMJ, we find that *rab11* is important for synaptic morphogenesis, as reductions in *rab11* function cause increases in bouton density and branching. These defects are also suppressed by loss of *bchs*. Taken together, these data identify Bchs as an antagonist of Rab11 during development and uncover a role for these regulators of vesicle trafficking in synaptic morphogenesis. This raises the interesting possibility that Bchs and other BEACH proteins may regulate vesicle traffic via interactions with Rab GTPases.

KEY WORDS: BEACH domain, Vesicle trafficking, Neuromuscular junction, Bouton, Bristle development, *Drosophila*

INTRODUCTION

BEACH proteins are conserved throughout eukaryotes. These large proteins, many of which exceed 400 kDa in size, have been implicated in cellular processes ranging from cytokinesis to synaptic transmission (Kwak et al., 1999; Su et al., 2004). Furthermore, mutations in several BEACH genes cause disease in humans. *LYST* (lysosomal trafficking regulator), the first BEACH gene to be discovered, is disrupted in Chédiak-Higashi syndrome – an often-fatal disease characterized by severe immunodeficiency, albinism, poor blood coagulation and neurologic involvement (Introne et al., 1999). Another BEACH family member, neurobeachin (NBEA), has been implicated as a candidate gene for autism (Castermans et al., 2003). Furthermore, upregulation of *LRBA* (LPS-responsive and beige-like anchor) is seen in several types of cancer and appears to facilitate cancer growth (Wang et al., 2004).

Localization of several BEACH proteins to subcellular membranes, as well as loss-of-function phenotypes that affect organelle morphology and function, suggest that these proteins may play roles in membrane trafficking. For instance, the hallmark of cells mutant in the *Lyst* gene is the presence of large intracellular granules of lysosomal origin, which probably result from increased lysosome fusion (Harris et al., 2002; Nagle et al., 1996). However, the mechanisms by which Lyst and other BEACH proteins regulate vesicle trafficking are not understood.

In the present study we have found a genetic interaction between *bchs* (blue cheese), a BEACH family member recently described in *Drosophila* (Finley et al., 2003), and *rab11*. The Rab family of small GTPases has a well-established involvement in membrane traffic; Rabs can regulate vesicle formation, motility, docking and fusion (Zerial and McBride, 2001). Rabs, like other GTPases, act as molecular switches: active in the GTP-bound form and inactive in the GDP-bound form. Moreover, each Rab must be associated with its particular subset of cellular membranes in order to carry out its function (Pfeffer and Aivazian, 2004; Seabra and Wasmeier, 2004). Thus, Rabs impart specificity to membrane trafficking events.

Rab11 localizes to the pericentriolar recycling endosome, the *trans*-Golgi network and post-Golgi vesicles (Chen et al., 1998; Ullrich et al., 1996), and plays a role in both the exocytic biosynthetic pathway and the recycling pathway (Chen et al., 1998; Ren et al., 1998; Satoh et al., 2005; Ullrich et al., 1996). In *Drosophila*, recent work has established a role for *rab11* in multiple developmental events, including polarization of the oocyte, cellularization of the embryo and morphogenesis of the rhabdomere, the photosensing organelle of photoreceptor neurons (Dollar et al., 2002; Pelissier et al., 2003; Riggs et al., 2003; Satoh et al., 2005). In addition, subcellular localization of Rab11 may contribute to asymmetric cell division (Jafar-Nejad et al., 2005).

In this paper we describe the characterization of *Drosophila* Bchs and its interaction with Rab11. We find that Bchs is highly expressed in the nervous system, where it is associated with vesicles and concentrated in synaptic regions. We show that reductions in *bchs* function suppress the effects of loss-of-function *rab11* mutations in multiple developmental contexts. In particular, *bchs* mutations suppress a newly described anatomical phenotype of *rab11* at the neuromuscular synapse. Our data identify a role for these regulators of vesicle trafficking in developmental events, such as synaptic morphogenesis, and provide insight into how BEACH proteins could be involved in vesicle trafficking.

MATERIALS AND METHODS

Fly stocks

EP lines (Rorth, 1996) were obtained from Rebay lab (Whitehead Institute, Cambridge, MA). *rab11*^{P2148}, *rab11*^{93Bi}, *Df(2L)cl7*, *pr[1] cn[1]/CyO*, and the *Drosophila* DK1, DK2 and DK3 deficiency kits (2001) were obtained from the Bloomington Stock Center, *rab11*^{ex1}*/TM3*, *Sb* and *rab11*^{ex2}*/TM3*, *Sb* from R. Cohen (University of Kansas). *w*, Canton S flies were use as control, unless otherwise indicated.

[1]Department of Biology, Massachusetts Institute of Technology, 77 Massachusetts Avenue 68-230B, Cambridge, MA 02139, USA. [2]Division of Neuroscience, Children's Hospital, Harvard Medical School, Boston, MA 02115, USA. [3]Biology Department, Brandeis University, MS-008, 415 South Street, Waltham, MA 02454, USA.

*Author for correspondence (e-mail: pgarrity@brandeis.edu)

Accepted 18 September 2006

In situ hybridization

Both sense and antisense RNA probes were made using DIG RNA labeling kit (Roche); the template was made by PCR from genomic fly DNA using the following primers: 5′-GAATTAATACGACTCACTAT-AGGGAGAGCACACAAAGTTCGATCTTGAC-3′ and 5′-AATTAAC-CCTCACTAAAGGGAGAGTTCGCCTACAAGCACATCG-3′. Embryo in situ hybridization was done as in Tautz and Pfeifle (Tautz and Pfeifle, 1989).

Mouse northern blot

Template for mouse RNA probe corresponding to 4737-5413 bp of *Wdfy3* cDNA was made by PCR from mouse cDNA (Gertler Laboratory, MIT), primers used 5′-T3CCTAAGCCTGTCGCCACTACTTTAC-3′ and 5′-T7CCAAACTTCTTCTTCTGCTCCCG-3′. Probe was synthesized using Strip-EZ RNA (Ambion) and a-P^{32}UTP 800 ci/mM (Amersham). Hybridization was done according to the manufacturer's instructions (Ambion).

EMS mutagenesis and sequencing of the *bchs* locus

Ethyl methanesulfonate (EMS) mutagenesis was performed as described (Lewis and Bacher, 1968). *bchs* alleles were PCR amplified from genomic DNA and sequenced by the MGH Core Facility. The following primers were used.

Pair 1: 5′-CAAACCCCACGGACATGC-3′ and 5′-GCTGGTGTG-GACTGACGCC-3′.

Pair 2: 5′-GCACGCTCCCTCCGTTCG-3′ and 5′-CAAACTTGGAG-CACTGCCTGAG-3′.

Pair 3: 5′-CAACCAGTTACAGGGTCGGAATC-3′ and 5′-GCGCT-GACCACTTTTGTAGTCTG-3′.

cDNA cloning and transgene constructs

Full-length *bchs* cDNA was assembled by combining a partial cDNA (clone LD02084) with cDNA produced via RT-PCR from S2 cell RNA (provided by Pardue Laboratory, MIT). RT (RETROscript, Ambion) and PCR (Expand High Fidelity PCR System, Roche) were done according to the manufacturer's instructions. The following primers were used: 5′-CGGGATCCATGAATGTAATGCGTAAGCTGCG-3′, 5′-CGGAATTC-GCCACCAAGGACTTGATGATTTCG-3′, 5′-CGGAATTCTGCTTCG-CACCACGCAGGTC-3′, 5′-CGGGATCCCGAGCGGACAACAAAAG-CATTG-3′, 5′-ACGCGTCGACCAGATTCCGACCCTGTAACTGG-3′, 5′-GCAACCACGAGTTGGAATTCATTGGC-3′ and 5′-ATTTGCGGC-CGCCCTAATTGTCCAACGAGTTCGTGC-3′.

Fragments were sequenced before assembly into full-length cDNA, which was modified with 5′ HA tag in pcDNA6/V5-His (Invitrogen) and inserted into pUASt (Brand and Perrimon, 1993).

Antibody production

Bchs aa 2237-2590 were expressed as 6XHis fusion protein in bacteria and purified according to the manufacturer's instructions (Amersham). Polyclonal antisera were produced in rats (Covance).

Western blotting

Each lane of a 6% SDS-polyacrylamide gel contained nine adult heads homogenized in 1× Laemmli buffer in PBS (130 mmol/l NaCl, 175 mmol/l Na_2HPO_4, 60 mmol/l NaH_2PO_4). After electrophoresis, proteins were transferred to Hybond-P membrane (Amersham Pharmacia) and membranes were blocked in 5% nonfat milk and probed with anti-Bchs (1:1000) and rat anti-Elav (1:1000), followed by HRP-conjugated goat anti-rat antibody (1:5000) (Jackson).

Immunohistochemistry

Immunohistochemistry of larval and adult brains was performed as previously described (Garrity et al., 1999). Anti-Bchs was preabsorbed using *bchs*^{17} animals and used at 1:500. Primary antibodies: mouse MAb 24B10 anti-Chaoptin (Fujita et al., 1982) (1:200), rabbit anti-Syt1 (T. Littleton, MIT) (1:500) and mouse anti-HA (Covance) (1:1000) were used. Secondary antibodies were goat anti-mouse HRP (1:200), goat anti-rat Cy3 (1:500), goat anti-rabbit FITC (1:200) and goat anti-mouse Cy3 (1:1000) (Jackson). Fluorescent samples were visualized using a Nikon PCM2000 confocal microscope.

Larval body wall dissections were done in PBS and fixed in 4% PFA in PBS. Anti-Bchs was preabsorbed using *bchs* null animals and used at 1:500. Mouse anti-Rab11 antibody (BD Biosciences) was used at 1:200. Subtracted goat anti-rat Cy3 at 1:100 (Jackson), goat anti-mouse Alexa-488 at 1:100. Cy5- and FITC-conjugated anti-HRP antibodies at 1:100 (Jackson) were used. Confocal data was acquired as single images or image stacks of multi-tracked, separate channels with a Zeiss LSM 510 microscope.

Screen for modifiers of Bchs overexpression

Each stock from the *Drosophila* Deficiency Kits (195 stocks that together delete over 85% of the genome) was crossed to *GMR-GAL4; EP-bchs* flies to determine whether heterozygosity for particular genomic region modified the adult eye phenotype caused by Bchs overexpression. Smaller deficiency chromosomes and mutations within genomic regions of interest were obtained (Bloomington Stock Center) and examined for interactions with *GMR-GAL4;EP-bchs*.

Quantification of survival and bristle phenotypes

To measure viability, 60 larvae (second instar) of each genotype were placed in identical vials at 25°C and monitored daily for survival to adulthood. Bristle loss was quantified by counting the numbers of bristle-filled and empty sockets in the last row of abdominal tergites (segments) 2, 3 and 4 in adults (≤1-day old). Fraction of bristle-filled sockets was calculated. At least ten animals per genotype were counted. All *P*-values were determined using two-tailed unpaired Student's *t*-tests.

Subcellular fractionation and western blotting

Sucrose gradient was prepared by Bill Adolfsen (Littleton Laboratory, MIT) as described in Adolfsen et al., 2004 (Adolfsen et al., 2004). Western blots were as described above using: rat anti-Bchs 1:1000, mouse anti-Rab11 (BD Biosciences) 1:1000, mouse anti-Rop (4F8) (Harrison et al., 1994) (H. Bellen, Baylor) 1:1000, and rabbit anti-Synaptotagmin (rabbit) (T. Littleton, MIT) 1:500. HRP-conjugated goat anti-rat, mouse, rabbit and guinea pig secondary antibodies (Jackson) were used at 1:5000.

Quantification of the bouton density and branching phenotypes

Confocal stacks through third instar NMJ 6/7 were flattened into projections using the LSM 510 software. Each bouton was marked on the image by a colored dot using Adobe Photoshop and the resulting dots were counted using ImageJ software. The number of branching boutons was counted in the same manner. Muscle surface area was estimated as described (Schuster et al., 1996).

RESULTS

Overexpression of *bchs* in photoreceptors causes abnormal growth cone morphology

We identified *bchs* in a genetic screen as a modifier of photoreceptor growth cone morphology when expressed at a high level in the retina. In this screen, we used a retina-specific promoter fused to GAL4 (*GMR-GAL4*) to overexpress genes adjacent to GAL4-responsive UAS elements. These genes were represented in a collection of about 2000 *Drosophila* lines that contained insertions of the UAS-bearing EP transposon (Rorth, 1996). One of these lines, EP(2)2299 (henceforth termed *EP-bchs*), contained an EP transposon insertion adjacent to *bchs*. When *bchs* was highly expressed in the developing retina by the *GMR-GAL4* driver, photoreceptor growth cones had an unusually bulbous central region and were less expanded than controls, although they appeared to grow normally toward their targets (Fig. 1A′,A″,B′,B″). While patterning of the third instar eye disc appeared normal in these *GMR-GAL4;EP-bchs* animals, suggesting that early eye development was not significantly affected (R.K., unpublished), overexpression of *bchs* in the retina resulted in a smaller, glazed adult eye (Fig. 1A,B).

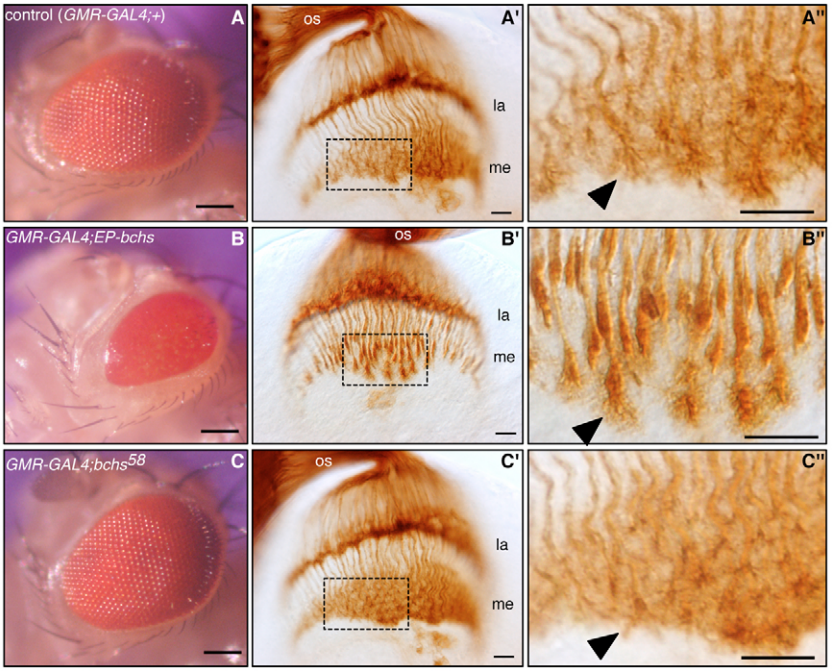

Fig. 1. Bchs overexpression disrupts eye development and photoreceptor growth cone morphology. (**A-C**) Adult eyes. (A) Control (*GMR-GAL4*) eye has normal rows of ommatidia. (B) Overexpression of wild-type Bchs in the eye (*GMR-GAL4;EP-bchs*) produces a small eye lacking distinct ommatidia. (C) An early stop codon in the *bchs*^{58} allele prevents the overexpression phenotype, despite the presence of the *EP-bchs* insertion in this allele (*GMR-GAL4;bchs*^{58}). (**A′-C′**) Photoreceptor (R-cell) axons in larval brain, labeled with anti-Chaoptin. Subsets of R-cell axons enter via the optic stalk to terminate in the lamina and medulla, from which the indicated region is enlarged in **A″-C″**. Compared with control brains (A′,A″), overexpression of wild-type Bchs (B′,B″) does not disrupt axon pathfinding, but causes photoreceptor growth cones (arrowheads) to have larger central areas and appear less expanded than controls. This phenotype is also prevented by the stop codon in *bchs*^{58} (C′,C″). Scale bars: 100 μm in A-C; 10 μm elsewhere. la, lamina; me, medulla; os, optic stalk.

Bchs is evolutionarily conserved and neuronally expressed

Bchs has a predicted mass of 390 kDa and has been evolutionarily conserved from the slime mold *Dictyostelium* to humans (De Lozanne, 2003). In all BEACH proteins, including Bchs, the BEACH domain is preceded by a pleckstrin-homology (PH) domain and followed by four to six WD40 repeats (five in Bchs) (Fig. 2A). The large size of most BEACH proteins combined with the presence of multiple WD40 domains, which serve as protein-protein interaction motifs, suggest that BEACH proteins could be involved in the assembly of large protein complexes. BEACH proteins have been subdivided into five classes (De Lozanne, 2003; Wang, N. et al., 2002). Whereas the PH-BEACH-WD40 module is conserved across the family, each BEACH protein has additional regions of homology particular to members of its class. There are five predicted BEACH proteins in *Drosophila*, and Bchs falls in a class that includes LvsA in *Dictyostelium*, several uncharacterized proteins in *Arabadopsis* and *Caenorhabditis elegans*, and two human members: Alfy (autophagy-linked FYVE protein; WDFY3 – Human Genome Nomenclature Database) and the uncharacterized molecule KIAA1607. Bchs has extensive homology to Alfy throughout the entire protein length: 51-84% amino acid identity in a carboxyl portion that includes the PH-BEACH-WD40 regions and 41% identity in the remainder of the protein, hereafter called CRAB (conserved region in Alfy and Bchs) (Fig. 2A). In addition to the PH-BEACH-WD40 module, Bchs and Alfy also have a C-terminal FYVE (Fab1p, YOTB, Vac1p and EEA1) domain (Fig. 2A), a motif that can mediate interactions with phosphatidylinositol 3-phosphate (Misra et al., 2001).

Both *bchs* and genes expressing the Alfy protein are expressed in the nervous system. RNA in situ hybridization indicated that *bchs* mRNA was enriched in, but not restricted to, the embryonic brain and ventral nerve cord (Fig. 2B) (see also Kraut et al., 2001). Similarly, transcripts for murine Alfy (*Wdfy3* – Mouse Genome Informatics) were expressed highly, but not exclusively, in the brain (Fig. 2C). Thus, Bchs and its homologs are neuronal, but are likely to also function in other cell types.

bchs mutants do not exhibit observable loss-of-function phenotypes

We reasoned that mutations disrupting *bchs* function would decrease or eliminate the ability of Bchs to alter the structure of the adult eye when overexpressed. Therefore, we mutagenized *EP-bchs* animals using EMS and isolated 17 independent *EP-bchs* chromosomes that no longer caused strong eye defects when combined with *GMR-GAL4* (Fig. 1 and Table 1). DNA sequencing identified mutations in the *bchs* gene in eight of these strains (Table 1). Examination of the larval photoreceptor axons in these animals showed that those mutations that strongly suppressed the adult eye phenotype also strongly suppressed the growth cone phenotype (Fig. 1C). The identification of these mutations within *bchs* not only provided loss-of-function *bchs* alleles for further analysis, but also confirmed that the growth cone and eye phenotypes resulted from *bchs* overexpression.

To characterize *bchs* alleles, we analyzed protein levels using antisera raised against amino acids 2237-2590 of Bchs, a region between the positions of the lesions in *bchs*^{13} and *bchs*^{17}. These antisera recognized a protein species migrating well above the 250 kDa marker on western blots, consistent with the predicted molecular weight for Bchs of 390 kDa (Fig. 2D). This protein species was increased in flies overexpressing *bchs* (*GMR-GAL4;EP-bchs*) and absent in flies homozygous for the *bchs* alleles *bchs*^{12}, *bchs*^{17}, and *bchs*^{58} (these alleles retain the EP transposon insertion present in *EP-bchs*). These data confirmed that the antibody detects Bchs protein and showed that three of our loss-of-function *bchs* alleles do not produce detectable full-length Bchs protein.

We examined multiple *bchs* alleles for mutant phenotypes, including the putative protein null alleles *bchs*^{12}, *bchs*^{17} and *bchs*^{58} in combination with a deficiency chromosome, *Df(2L)cl7*, missing the *bchs* locus. Mutants in *bchs* were viable, fertile and had no overt defects. Furthermore, no defects in axon guidance or growth cone morphology could be detected in the larval visual system or the embryonic central nervous system (CNS) and motor axons (R.K., unpublished).

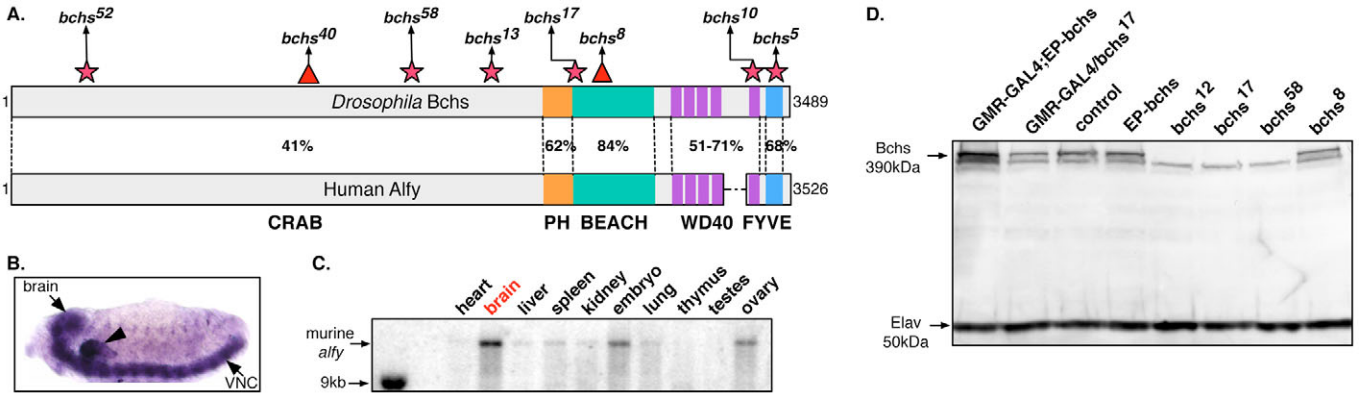

Fig. 2. Structure and expression of Bchs protein. (**A**) The domains of *Drosophila* Bchs and human Alfy are similar in organization and sequence. The percentage amino acid identity between domains is indicated, including homology for the extended portion of the protein called CRAB (Conserved Region in Alfy and Bchs; shown in gray and not shown to scale to conserve space). Mutations in *bchs* alleles are marked (nonsense, stars; missense, triangles). (**B**) In a stage 13 embryo, *bchs* mRNA is highly expressed in embryonic CNS, including brain and ventral nerve cord, and in the salivary glands (arrowhead). A sense control probe showed no signal above background (data not shown). (**C**) Analysis of murine mRNA indicates mouse Alfy is widely expressed, but enriched in adult brain. (**D**) Protein blot probed with antisera raised to amino acids 2237-2590 of Bchs (arrow indicates Bchs; just below Bchs, the anti-sera also detects a crossreacting protein, whose size and intensity are unaffected in multiple *bchs* truncation alleles). *GMR-GAL4;EP-bchs* animals express more Bchs protein than controls, including *EP-bchs*. Overexpression is abolished by the nonsense mutation in $bchs^{17}$ (*GMR-GAL4;*$bchs^{17}$/+). $bchs^{12}$, $bchs^{17}$ and $bchs^{58}$ express no detectable Bchs, while $bchs^{8}$ still produces substantial amounts of protein. Antibody against Elav demonstrates equal loading. VNC, ventral nerve cord.

rab11 is a modifier of Bchs overexpression

To gain insight into the function of Bchs, we searched for genes that could alter the adult eye phenotype caused by Bchs overexpression. We examined a collection of 195 chromosomal deficiencies that deleted defined portions of the *Drosophila* genome (in total, covering ≈85% of the genome). Five chromosomal deficiencies dominantly suppressed the *GMR-GAL4;EP-bchs* eye phenotype, while eight dominantly enhanced it. In particular, deficiency *Df(3R)e-R1* acted as a strong enhancer. Genes within the interval deleted by *Df(3R)e-R1* were examined, and mutations in *rab11* were found to strongly enhance the Bchs overexpression phenotype (Fig. 3). Multiple loss-of-function *rab11* alleles were tested, including $rab11^{ex1}$, $rab11^{ex2}$, $rab11^{E(To)3}$, $rab11^{E(To)11}$ and $rab11^{J2D1}$(also known as $rab11^{P2148}$) (Dollar et al., 2002; Jankovics et al., 2001). Heterozygocity for *rab11* did not cause a disruption in eye development in otherwise wild-type animals, but all the examined *rab11* mutants showed a strong dominant enhancement of the *bchs* overexpression phenotype (Fig. 3). Thus, Bchs overexpression makes the eye sensitive to partial reductions in *rab11* gene function, raising the possibility that Bchs and Rab11 functionally antagonize one another.

Loss of *bchs* suppresses *rab11* lethality

As decreased dosage of *rab11* enhanced the Bchs overexpression phenotype, we wanted to test whether the loss of *bchs* would, in turn, suppress *rab11* loss-of-function phenotypes. Null *rab11* mutants die in mid-embryogenesis; however, *rab11* hypomorphs exhibit different degrees of lethality, sterility and bristle defects (Dollar et al., 2002; Jankovics et al., 2001). The combination of a hypomorphic allele $rab11^{93Bi}$ and a putative null allele $rab11^{ex1}$ (Dollar et al., 2002) is mostly lethal (Jankovics et al., 2001), but a small number of $rab11^{ex1}$/$rab11^{93Bi}$ flies survive to adulthood. To test whether the

Table 1. Selected *bchs* alleles

Allele number	Molecular lesion	Type of mutation and domains affected	Bchs protein level	Suppression of adult eye
$bchs^{104}$	?	?	Low	Weak
$bchs^{105}$	Q_{3428}-Stop	Truncation: removes most of the FYVE domain	Low	Weak
$bchs^{8}$	T_{2656}-I	Missense mutation in the BEACH domain: affects the predicted PH-BEACH interface	Approx. 50% of control	Strong
$bchs^{10}$	W_{3406}-Stop	Truncation: removes the FYVE domain	Very low	Strong
$bchs^{12}$	?	?	Undetectable	Strong
$bchs^{13}$	W_{2217}-Stop	Truncation: removes the PH, BEACH, WD40, FYVE domains	Very low	Strong
$bchs^{17}$	W_{2640}-Stop	Truncation: removes most of the BEACH, all of the PH, WD40 and FYVE domains	Undetectable	Strong
$bchs^{26}$	?	?	Undetectable over deficiency	Strong
$bchs^{40}$	G_{1224}-D	Missense mutation in CRAB	Very low	Strong
$bchs^{43}$	?	?	Undetectable over deficiency	Strong
$bchs^{52}$	Q_{410}-Stop	Early Stop, appears to have some read-through the Stop codon	Very low	Strong
$bchs^{58}$	I_{1830}...Stop	Truncation: removes the PH, BEACH, WD40, FYVE domains	Undetectable	Strong

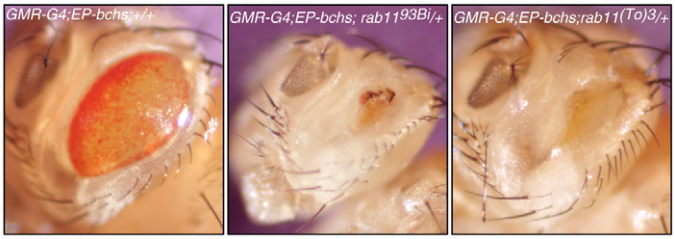

Fig. 3. Reductions in *rab11* enhance the *bchs* overexpression phenotype. (Left) Bchs overexpression produces a small, glazed eye. (Middle, right) Heterozygosity for *rab11* alone has no eye phenotype (not shown) but further reduces the eye in animals that overexpress Bchs.

loss of *bchs* had an effect on the viability of $rab11^{ex1}/rab11^{93Bi}$ mutants, we introduced into this genotype the putative protein null alleles $bchs^{12}$, $bchs^{17}$ and *Df(2L)cl7*. Loss of one or both copies of *bchs* strongly enhanced the viability of $rab11^{ex1}/rab11^{93Bi}$ animals (Fig. 4A,B). For example, in one experiment, survival to adulthood was improved from 17±4% in $rab11^{ex1}/rab11^{93Bi}$ mutants to 77±3% in $bchs^{12}/bchs^{17};rab11^{ex1}/rab11^{93Bi}$ double mutants (all values are mean±s.e.m., n=3 independent vials, P<0.001) (Fig. 4A). In another experiment, survival was improved from 5±1% for $rab11^{ex1}/rab11^{93Bi}$ mutants to 48±6% for $bchs^{17}/+;rab11^{ex1}/rab11^{93Bi}$ animals (n=8 independent vials, P<0.001) (Fig. 4B). Thus, reduction in, or loss of, *bchs* function increases the survival of *rab11* mutants. This suggests that Bchs antagonizes essential functions of Rab11.

Loss of *bchs* suppresses *rab11* bristle defects

The posterior abdomens of viable *rab11* mutants are missing many small mechanosensory bristles (or microchaetae) (Fig. 5A) (Jankovics et al., 2001). In addition, the posterior scutellar macrochaetae, large mechanosensory bristles, are shortened in $rab11^{ex1}/rab11^{93Bi}$ mutants (Fig. 5B). Mutations in *bchs* suppressed both the bristle shortening and the bristle loss defects of *rab11* mutants (Fig. 5A,B). To quantify this suppression we calculated the fraction of empty sockets in the last row of abdominal tergites 2, 3 and 4 for two different allelic combinations of *rab11* (the viable $rab11^{93Bi}$ homozygote and the semi-lethal $rab11^{ex1}/rab11^{93Bi}$ heterozygote) alone and in combination with *bchs* alleles. Reductions in *bchs* suppressed bristle loss in both *rab11* allelic combinations in a dosage-dependent manner. The removal of one copy of *bchs* strongly suppressed bristle loss, and the removal of both copies returned the number of bristles to control levels (Fig. 5C). As expected from the western blot above, $bchs^{17}$ and $bchs^{12}$ were indistinguishable in this suppression assay from *Df(2L)cl7*, suggesting that they are null alleles. These data further support the conclusion that Bchs and Rab11 function antagonistically during *Drosophila* development.

Interestingly, $bchs^{8}$, which produces full-length Bchs protein, suppressed bristle loss to the same extent as the protein null $bchs^{58}$ allele (Fig. 5C, bottom panel). This suggests that the missense mutation in $bchs^{8}$, which alters a conserved threonine in the interface between the PH and the BEACH domains of the protein (Fig. 2A and Table 1) (Jogl et al., 2002), strongly disrupts protein function.

Bchs and Rab11 proteins localize to overlapping membrane regions

We examined the localization of Bchs protein in the larval brain and found that it was enriched in synaptic regions within the CNS (Fig. 6A). The specificity of the Bchs immunoreactivity was demonstrated by its absence from the neuropil of $bchs^{12}$.

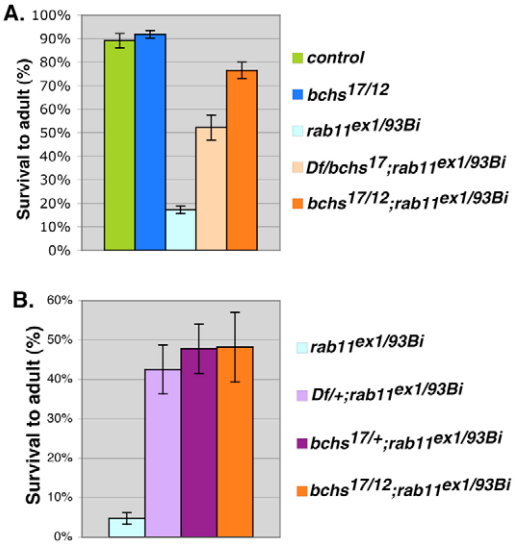

Fig. 4. *bchs* mutations suppress the lethality of *rab11* mutants. Sixty second-instar larvae of each genotype were placed in identical vials and monitored for survival to adulthood. *Df* is *Df(2L)cl7*, a chromosome deleted for *bchs*. Data in A and B represent two independent sets of experiments that were not pooled because the survival of *rab11* mutants varied slightly between them. (**A**) *bchs* mutations reduce lethality of *rab11* hypomorphs (P<0.01 for $Df(2L)cl7/bchs^{17};rab11^{ex1}/rab11^{93Bi}$ vs $rab11^{ex1}/rab11^{93Bi}$ and P<0.0005 for $bchs^{17}/bchs^{12};rab11^{ex1}/rab11^{93Bi}$ vs $rab11^{ex1}/rab11^{93Bi}$) (n≥3 vials/genotype, unpaired t-test). (**B**) Two-fold reduction in *bchs* gene dosage reduces lethality of *rab11* hypomorphs. Compared to $rab11^{ex1}/rab11^{93Bi}$: P<0.005 for $Df(2L)cl7/+;rab11^{ex1}/rab11^{93Bi}$, P<0.0005 for $bchs^{17}/+;rab11^{ex1}/rab11^{93Bi}$ and P<0.01 for $bchs^{17}/bchs^{12};rab11^{ex1}/rab11^{93Bi}$ (n≥5 vials/genotype). Error bars are s.e.m.

To examine the distribution of Bchs protein within a neuron at greater resolution, we expressed an HA-tagged version of full-length Bchs in ellipsoid body neurons using *EB1-GAL4* (Wang, J. et al., 2002). EB neurons extend a single neurite that splits into distinct dendritic and axonal processes, with the dendrite arborizing in the lateral triangle, and the axon in the ellipsoid body ring (Hanesch et al., 1989). Whereas a membrane-associated CD8-GFP fusion (Chang et al., 2002) was evenly distributed throughout these neurons, HA-Bchs preferentially accumulated near the axon terminals (Fig. 6B), suggesting that Bchs can preferentially localize to the presynaptic regions of a neuron.

The larval neuromuscular junction (NMJ) provides the opportunity to examine individual synaptic terminals isolated from other neuronal elements. In these preparations, some Bchs immunoreactivity was present in the muscle fibers, but it was most prominent within the nerve terminals (Fig. 6C,D). Bright puncta of Bchs immunoreactivity were observed presynaptically, as was established by using anti-HRP to label the surrounding neuronal plasma membrane. In double-labeling experiments, the Bchs-immunoreactive puncta failed to correlate with other subcellular compartments that have been characterized at the NMJ, including early endosomes marked with 2XFYVE-GFP and Rab5-GFP (Wucherpfennig et al., 2003), dense-core vesicles marked with ANF-GFP (Rao et al., 2001) and recycling vesicles marked with Clathrin-GFP (Chang et al., 2002) (Fig. 7A,B,C,D, respectively).

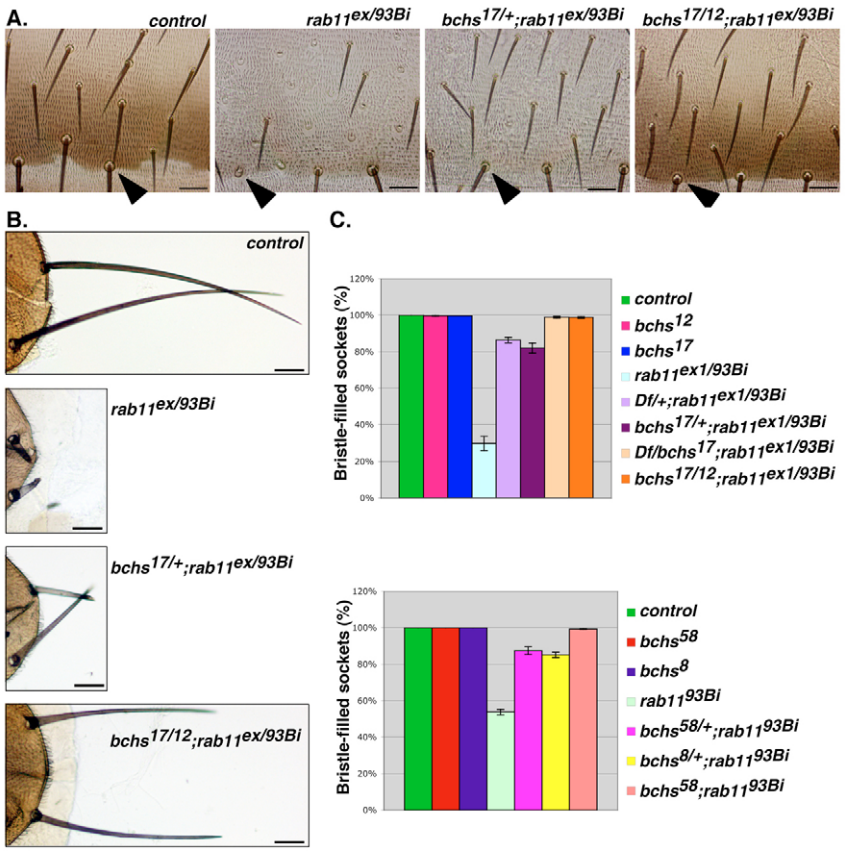

Fig. 5. *bchs* mutations suppress bristle defects of *rab11* mutants. (**A**) Portions of posterior abdomens from indicated genotypes. In control, each socket contains a bristle (microchaete), but in $rab11^{ex1}/rab11^{93Bi}$ many sockets are empty. Mutation of one copy of *bchs* ($bchs^{17}/+;rab11^{ex1}/rab11^{93Bi}$) restores many bristles, while mutation of both copies of *bchs* ($bchs^{17}/bchs^{12};rab11^{ex1}/rab11^{93Bi}$) restores all bristles. Arrowheads indicate bristle-filled or empty sockets in the last row of the third abdominal tergite (segment). (**B**) Portions of posterior scutellum from indicated genotypes. Posterior scutellar bristles are shortened in $rab11^{ex1}/rab11^{93Bi}$. Bristle length is restored partially by one mutant copy of *bchs* ($bchs^{17}/+;rab11^{ex1}/rab11^{93Bi}$) and more fully by homozygosity for *bchs* ($bchs^{17}/bchs^{12};rab11^{ex1}/rab11^{93Bi}$). (**C**) Quantitation of abdominal bristle loss. The fraction of sockets containing bristles was calculated for the last row of abdominal tergites 2, 3 and 4. Error bars are s.e.m. *Df* is *Df(2L)cl7*, a chromosome deleted for *bchs*. Top panel: reduction of *bchs* gene dosage suppresses bristle loss of $rab11^{ex1}/rab11^{93Bi}$. $n \geq 10$ for each genotype, $P<0.0001$ for all genotypes compared to $rab11^{ex1}/rab11^{93Bi}$. Bottom panel: reduction of *bchs* gene dosage suppresses bristle loss of $rab11^{93Bi}$ homozygotes. $n \geq 10$ for each genotype, $P<0.0001$ for all genotypes compared to $rab11^{93Bi}/rab11^{93Bi}$. Scale bars: 30 μm in A; 50 μm in B.

Rab11 immunoreactivity had not been previously characterized at the NMJ; therefore, we examined its distribution to determine whether it, like Bchs, was enriched at the synapse. Rab11-positive puncta were present in nerves, synaptic boutons and muscles (Fig. 8A). The observed staining was specific for Rab11, as it was greatly reduced in $rab11^{ex1}/rab11^{93Bi}$ mutants, which also showed reduced protein levels (compared with controls) by western blot analysis (Fig. 8A,B). While both Rab11 and Bchs labeled puncta at the NMJ, Bchs was more enriched in the boutons than Rab11, while Rab11 was more abundant in the muscles than Bchs. Double labeling these preparations for Rab11 and Bchs demonstrated that their subcellular localization substantially overlapped both in neurons and muscle cells (Fig. 8C), although some puncta were immunoreactive for only one protein or the other. Within puncta that contained both proteins, Bchs and Rab11 staining was not always perfectly congruent: Bchs immunoreactivity at times predominated to one side of the stained structure and Rab11 to the other (Fig. 8C, arrows). These localization data, showing that Bchs and Rab11 are present in overlapping locations at the NMJ, together with the genetic interaction data, suggest that Bchs and Rab11 function in the same or closely related processes.

The results of biochemical fractionation experiments were also consistent with the partially overlapping distribution of Bchs and Rab11 proteins detected by immunohistochemistry at the NMJ. We probed fractions [previously characterized in Adolfsen et al. (Adolfsen et al., 2004)] from a 10-30% sucrose velocity gradient of head extract to determine how Bchs migrated with respect to known membrane fractions (Fig. 9). Bchs migrated with an intermediate density characteristic of a membrane-associated protein, but did not co-migrate with either the plasma membrane marker Syntaxin 1A (Schulze et al., 1995) or the synaptic vesicle markers neuronal-Synaptobrevin and Synaptotagmin1 (DiAntonio et al., 1993; Littleton et al., 1993). Rab11 showed a different distribution across the gradient than Bchs (Fig. 9). Nonetheless, a significant amount of Rab11 was recovered in fraction 17, the fraction in which Bchs was most abundant. Such partial co-migration of Bchs and Rab11 is consistent with localization of these proteins to partially overlapping membrane compartments.

Loss of *bchs* suppresses a *rab11* NMJ phenotype

Given the genetic interactions between *bchs* and *rab11* observed elsewhere in the animal, and the overlap of Bchs and Rab11 protein distribution at the NMJ, we investigated whether *rab11* and *bchs* interacted in NMJ development. We compared the phenotype of the hypomorph $rab11^{ex1}/rab11^{93Bi}$ to controls, with and without *bchs*, using the null genotype $bchs^{17}/bchs^{12}$. Although overexpression of Bchs causes bulges at the junctions between the axons and the synaptic branches (Kraut et al., 2001), *bchs* loss-of-function mutants had no detectable defects at the NMJ. *rab11* hypomorphs, however, showed significant alterations in synaptic bouton patterning at all NMJs. The defect was quantified at the muscle 6/7 synapse in abdominal segment A3, where the total number of synaptic boutons increased by ≈60% in *rab11* mutants compared with controls (166±11 versus 98±5, n=14 for each genotype; mean±s.e.m.; $P<0.0001$). Because synapses at the NMJ of wild-type larvae grow in proportion to muscle size (Schuster et al., 1996), we also calculated the number of boutons per unit of estimated muscle area. When the decreased size of *rab11* muscles was taken into account ($50\pm2\times10^3$ μm^2 in *rab11* versus $67\pm1\times10^3$ μm^2 in control), the density of synaptic boutons/μm^2 muscle area in the mutants was more than double that of controls ($3.3\pm0.2\times10^{-3}$ versus $1.5\pm0.1\times10^{-3}$ boutons/μm^2; n=14; $P<0.0001$) (Fig. 10A,B).

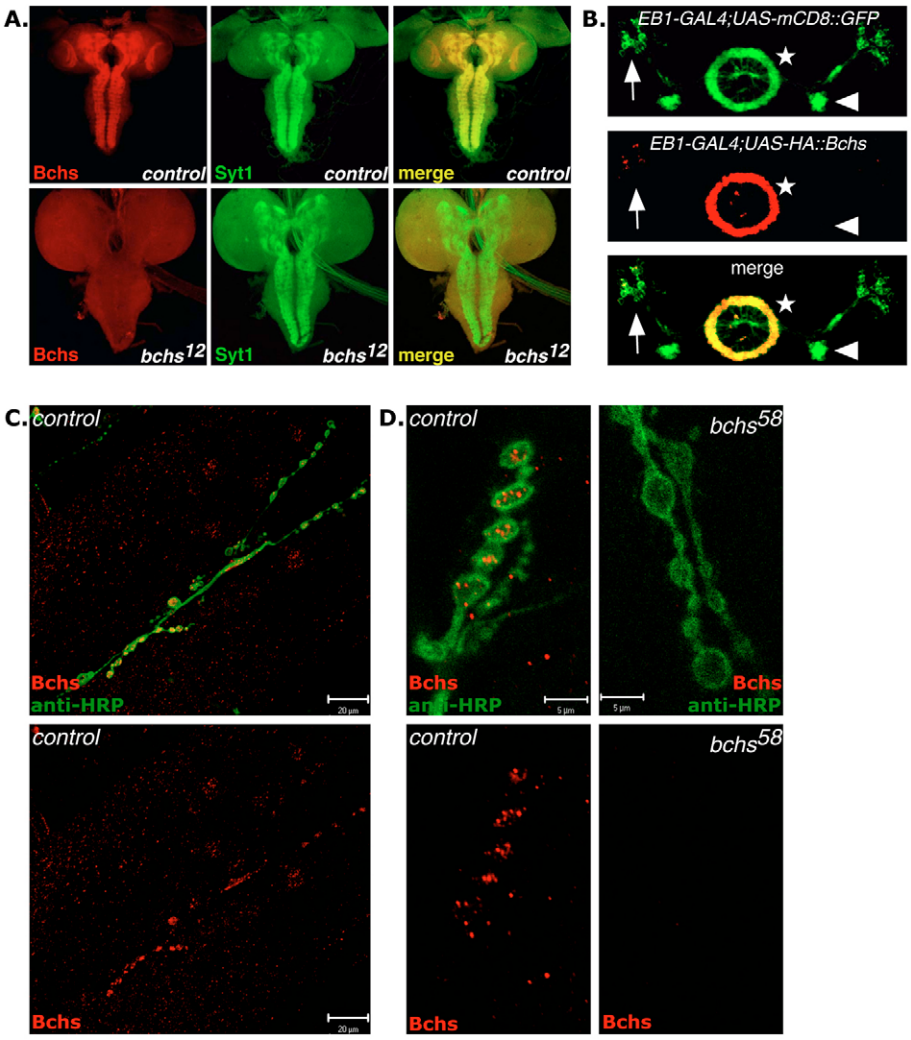

Fig. 6. Bchs localization in presynaptic endings. (**A**) Bchs immunoreactivity (red) within the third-instar larval brain and nerve cord is enriched in the synaptic neuropil, marked with Synaptotagmin1 immunoreactivity (green). Bchs immunoreactivity is undetectable in *bchs*^{12}. (**B**) When expressed in the adult ellipsoid body, HA-tagged Bchs (red) accumulates in the axon terminals of EB neurons, while transmembrane mCD8::GFP (green) distributes evenly throughout these neurons. Stars denote EB neuron presynaptic terminals, arrowheads point to EB neuron dendrites, arrows point to EB cell bodies. (**C**) In a confocal stack of images from a third-instar NMJ (muscle 6/7), Bchs immunoreactivity (red) is enriched in synaptic boutons. The neuronal membrane is outlined by anti-HRP (green). (**D**) In a single confocal section, Bchs puncta (red) are visible within the HRP-labeled (green) neuronal ending. The specificity of this immunoreactivity is confirmed by its absence in *bchs*^{58}. Scale bars: 20 μm in C; 5 μm in D. EB, ellipsoid body.

In addition to the increase in number and density, the boutons in *rab11* mutants were often arrayed in tight clusters resembling bunches of grapes, rather than the normal beads-on-a-string morphology. Among the previously described phenotypes at the NMJ, *rab11* most closely resembled that of *nervous wreck*, a mutation influencing the WASP signaling pathway (Coyle et al., 2004). The unusual clustering of boutons in *rab11* mutants was related to an increase in the number of branching boutons – those connected to more than two neighboring boutons. Normally such branch points are uncommon, but in *rab11* mutants the fraction of boutons that branch increased 2.6-fold (22.2±0.8% of all boutons versus 8.4±0.4% in control; n=14; P<0.0001) (Fig. 10A,B). Thus, *rab11* mutants are abnormal in synaptic growth and morphogenesis.

The NMJ phenotypes observed in *rab11* mutants were partially suppressed by loss-of-function mutations in *bchs*. Muscle size was restored to near control in *bchs,rab11* double mutant animals ($64\pm3\times10^3$ μm^2 in *bchs;rab11* vs. $67\pm1\times10^3$ μm^2 in control, n=14). The *bchs,rab11* double mutant and *rab11* single mutant had similar numbers of synaptic boutons. However, the density of boutons per muscle area in *bchs,rab11* animals was significantly less than in *rab11* mutants alone ($2.5\pm0.2\times10^{-3}$ boutons/μm^2; 169% of control in *bchs,rab11* versus $3.3\pm0.2\times10^{-3}$ boutons/μm^2; 225% of control in *rab11*; n=14, P<0.01). This represents a 44% suppression of the *rab11* phenotype (Fig. 10A,B). The percentage of branching boutons in the *bchs,rab11* double mutant was also significantly less than in *rab11* alone (15.6±1.1% versus 22.2±0.8%; n=14; P<0.0001). This represents a 48% suppression of the *rab11* phenotype (Fig. 10A,B). Thus, loss of *bchs* partially suppressed the increases both in bouton density and in bouton branching exhibited by *rab11* mutants. Consequently, Bchs probably has a modulatory role in synaptic development, acting as an antagonist of Rab11.

DISCUSSION

Bchs and Rab11 interact in intracellular traffic

While several BEACH-family proteins have been implicated in vesicle trafficking, the mechanisms through which they may regulate this process are unknown. We have shown that Bchs, the *Drosophila* relative of the human Alfy protein, is a functional antagonist of the vesicle-trafficking regulator Rab11. In particular, reduction in *bchs* strongly suppressed the defects in viability, synaptic morphogenesis and bristle extension exhibited by *rab11* loss-of-function mutants. Additionally, reduction in *rab11* activity strongly enhanced the eye phenotype caused by *bchs* gain of function. The reciprocity of genetic interactions between these two genes provides compelling evidence that Bchs participates in many of the same processes as Rab11 and, thus, suggests that Bchs, like Rab11, is a regulator of vesicle trafficking.

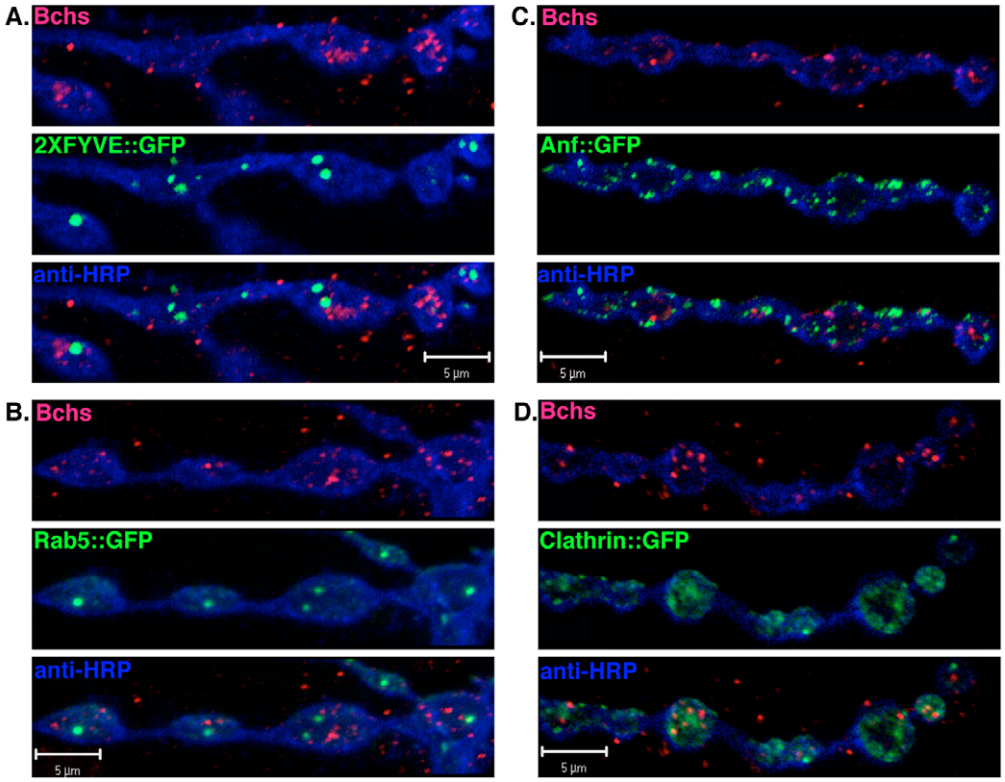

Fig. 7. Bchs localizes to a distinct compartment within presynaptic terminals at the NMJ. All GFP-tagged markers (green) were expressed using a pan-neuronal Elav-GAL4 driver. anti-HRP immunoreactivity (blue) marks the neuronal membrane. Bchs-immunoreactive puncta (red) do not show significant overlap with (**A**) 2XFYVE-GFP or (**B**) Rab5-GFP, which mark the early endosomal compartment (Wucherpfennig et al., 2003), (**C**) Anf-GFP, a dense-core vesicle marker, or (**D**) resemble the periactive zone staining of Clathrin-GFP, which marks areas actively undergoing endocytosis. A single confocal section at NMJ 6/7 is show in each panel. Scale bars: 5 μm.

The subcellular localization of Bchs also supports the hypothesis that this protein functions in membrane traffic. Bchs was present exclusively in membrane fractions and exhibited punctate staining in the presynaptic motoneuron terminals and in the muscles at the NMJ. This pattern is consistent with the localization of Bchs to a membrane-bound organelle. Furthermore, in line with a functional relationship between Bchs and Rab11, we observed significant subcellular co-localization of Bchs and Rab11 at the NMJ, as well as partial overlap in the distribution of Bchs and Rab11 within membrane fractions. These data further support our hypothesis that Bchs regulates vesicle trafficking and that it may do so via an interaction with the Rab11 GTPase.

Bchs modulates Rab11-dependent processes that involve membrane traffic

A prominent *bchs* phenotype was the suppression of the *rab11* sensory bristle defects, which entailed both shortened and missing bristles. These defects probably arose from alterations in membrane traffic. The extension of sensory bristles involves several vesicle trafficking steps, including membrane addition at the tip of the growing bristle and the secretion of cuticle to support the bristle cell. The complete loss of mechanosensory bristles could result from extremely impaired bristle growth. Alternatively, bristle loss could arise from a cell fate transformation that prevents the specification of the bristle-producing cell, as Rab11-mediated vesicle trafficking has also been implicated in the asymmetric cell divisions of the precursors that give rise to these cells (Jafar-Nejad et al., 2005). The ability of mutations in *bchs* to strongly suppress all *rab11* bristle defects implicates Bchs in bristle morphogenesis and is consistent with it playing a role in Rab11-mediated vesicle trafficking.

We have also uncovered a crucial role for *rab11* in the formation of the *Drosophila* NMJ: *rab11* mutants exhibit an increase in the density and branching of synaptic boutons and a decrease in the size of the muscles. Vesicle trafficking is important in determining the number and morphology of boutons at the NMJ (Dickman et al., 2006). In sculpting the synapse, membrane traffic is needed not only for the addition of new membrane and active zone proteins, but also for the insertion, removal and signaling of regulatory molecules at the cell surface (Marie et al., 2004; Sweeney and Davis, 2002). Furthermore, exocyst-dependent membrane addition is required for the expansion of NMJs (Murthy et al., 2003), and Rab11 is a known regulator of exocyst function (Beronja et al., 2005; Zhang et al., 2004). Thus, Rab11 is involved in synaptic morphogenesis at the NMJ, probably via regulation of vesicle trafficking.

By virtue of suppressing *rab11* NMJ phenotypes, Bchs is also implicated in a membrane-trafficking aspect of synaptic morphogenesis. Consistent with such a model, both Bchs and Rab11 showed punctate localization and partial overlap at the NMJ. A functional role of Bchs in presynaptic development may explain its concentration in the axonal rather than dendritic compartment of ellipsoid body neurons (Fig. 7B).

Membrane pathways modulated by Bchs

The link between Bchs and Rab11 function provides initial mechanistic insights into the trafficking pathways that may involve Bchs. Rab11 is involved in both biosynthetic exocytic traffic and membrane traffic through the recycling endosome (Pelissier et al., 2003; Satoh et al., 2005). As the loss of *bchs* suppresses lethality of *rab11* alleles, it is likely to be involved in all the essential functions of Rab11.

The partial colocalization of Bchs and Rab11 suggests candidate sites for the function of Bchs. In particular, Rab11 has been observed on the *trans*-Golgi network, post-Golgi vesicles, recycling endosomes and vesicles that travel from the recycling endosome to the plasma membrane (Chen et al., 1998; Ullrich et al., 1996; Ward et al., 2005). In regulating traffic to the plasma membrane, Rab11

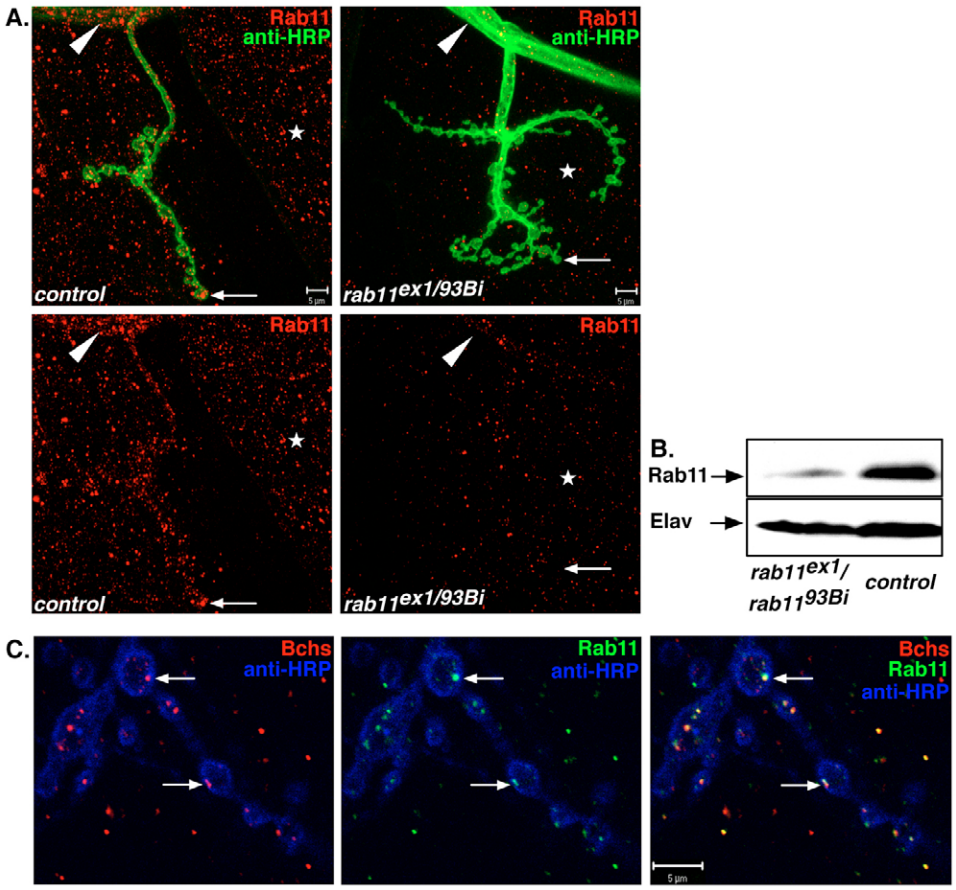

Fig. 8. Bchs and Rab11 partially overlap within the NMJ. (**A**) Rab11 positive puncta are present in the motor axon (arrowhead), synaptic boutons (arrow) and muscle (star). The number and brightness of Rab11 puncta are reduced in $rab11^{ex1}/rab11^{93Bi}$ hypomorph (right panels) compared with control (left panels). Confocal stacks through NMJs at muscle 4 are shown. (**B**) $rab11^{ex1}/rab11^{93Bi}$ mutants have reduced levels of Rab11 protein compared with controls. Anti-Elav serves as control for protein loading. (**C**) Single confocal slice through muscle 4 NMJ of third instar larva, double labeled for Rab11 (green) and Bchs (red), reveals significant overlap. Anti-HRP (blue) outlines neuronal membrane. Scale bars: 5 μm.

has been shown to physically interact with members of the exocyst complex (Beronja et al., 2005; Zhang et al., 2004). We found the distribution of Bchs to be highly polarized in neurons and enriched at synaptic endings, not cell bodies or dendrites. This suggests that interactions between Bchs and Rab11 may occur in a compartment adjacent to the presynaptic plasma membrane, rather than near the *trans*-Golgi network, the perinuclear recycling endosome or dendritic endosomes.

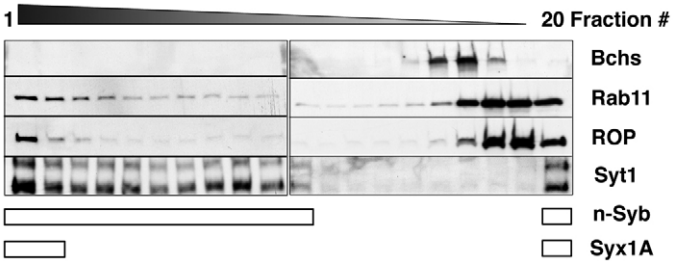

Fig. 9. Bchs and Rab11 partially co-fractionate in membrane preparations. Post-nuclear fractions of Canton S head extracts were fractionated on a 10-30% sucrose gradient and characterized in Adolfsen et al. (Adolfsen et al., 2004). (**A**) Synaptic vesicle fractions were detected with anti-Synaptotagmin1 (Syt1) antibody. Bchs and Rab11 localize to partially overlapping fractions (15-18). Unlike Rab11, Bchs was not present in the plasma membrane (fraction 1; containing ROP and syntaxin) or Syt1-positive synaptic vesicle fractions. Fractions positive for the plasma membrane marker Syx1A and synaptic vesicle marker n-Syb, as published in Adolfsen et al. (Adolfsen et al., 2004), are marked.

At the synapse, the most prominent membrane trafficking pathway is the synaptic vesicle cycle. However, Bchs immunoreactivity did not colocalize with synaptic vesicles or co-migrate with them in cell fractionation. These findings, together with the fact that loss of *bchs* does not alter the viability of the mutants, suggests that Bchs does not play a major role in the release of neurotransmitter. In this regard, Bchs is clearly distinct from Neurobeachin, a Beach-domain protein that is essential for transmitter release at the mouse NMJ (Su et al., 2004). Bchs did not colocalize with early endosomes, marked with either 2XFYVE-GFP or Rab5-GFP, through which at least some synaptic vesicles are thought to cycle, nor did Bchs immunoreactivity resemble the distribution of endocytic vesicles identified by clathrin-GFP. The former was perhaps surprising, given that Bchs possesses a FYVE domain. These data suggest that Bchs is unlikely to be involved in early endocytic events. The BEACH domain protein Lyst has been implicated in lysosomal trafficking; however, we observed no overlap of Bchs immunoreactivity with lysotracker (R.K., unpublished). Bchs is, therefore, not a lysosomal protein. Rather, Bchs appears to reside on a novel synaptic compartment adjacent to or overlapping a Rab11-containing organelle. We speculate that this may be a previously unappreciated presynaptic sorting endosome through which either recycled or Golgi-derived proteins are trafficked.

The nature of the Bchs-Rab11 interaction

What cellular and molecular mechanisms underlie the extensive genetic interactions between *bchs* and *rab11*? In one scenario, Bchs could negatively regulate Rab11 activity, perhaps by promoting a Rab11-GAP that restricts Rab11 function. Bchs could modulate the

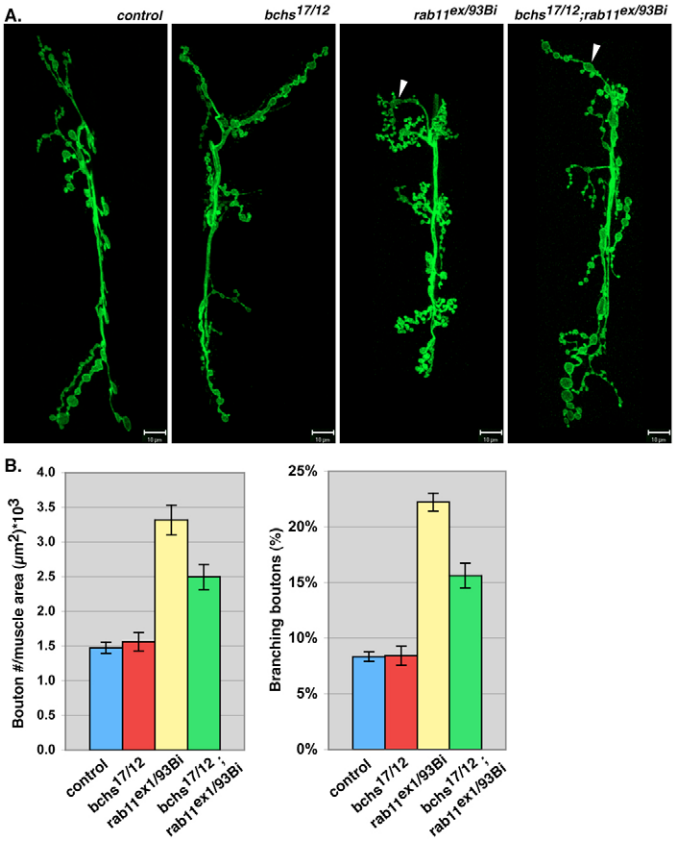

Fig. 10. *rab11* mutants have a morphological phenotype at the NMJ that is suppressed by *bchs*. (**A**) Confocal images of muscle 6/7 of abdominal segment 3 labeled with anti-HRP to outline neuronal membrane. Compared with controls and *bchs* mutants, $rab11^{ex1}/rab11^{93Bi}$ animals have an increased density of synaptic boutons and an increased percentage of boutons that are branched (connected to three or more adjacent boutons; arrowheads). Both defects are suppressed in $bchs^{17}/bchs^{12};rab11^{ex1}/rab11^{93Bi}$ double mutants. (**B**,**C**) Quantification of *bchs*-dependent *rab11* NMJ defects in bouton density (B) and branching (C). Bouton density (bouton number/μm^2 muscle area) in $rab11^{ex1}/rab11^{93Bi}$ mutants is 225% of control (P<0.0001). This defect is suppressed in $bchs^{17}/bchs^{12};rab11^{ex1}/rab11^{93Bi}$ double mutants (P<0.01 compared to $rab11^{ex1}/rab11^{93Bi}$). In $rab11^{ex1}/rab11^{93Bi}$ mutants, the fraction of branching boutons is 266% of control (P<0.0001). This defect is also suppressed in $bchs^{17}/bchs^{12};rab11^{ex1}/rab11^{93Bi}$ double mutants (P<0.0001 compared to $rab11^{ex1}/rab11^{93Bi}$). n=14 for each genotype. Scale bars: 10 μm.

efficacy of Rab11 function, but might be only one of several negative regulators of Rab11. Such a model would be consistent with our genetic studies, as loss of *bchs* might not cause defects on its own, but *bchs* overexpression would shut down the Rab11 pathway. Alternatively, *rab11* and *bchs* could be involved in competing intracellular pathways. For example, Rab11 might direct endosomal cargos toward the plasma membrane, while Bchs diverts these cargos elsewhere. This hypothesis receives support from the observation that Rab11 and Bchs appear to concentrate in partially distinct subcompartments of those organelles on which they both reside (Fig. 8C). This pattern of partially overlapping localizations is reminiscent of other pairs of regulators of membrane traffic, including Rab4 and Rab5, and Rab4 and Rab11 on two sequential, yet distinct, populations of endosomes. The distribution of these Rabs reflects their participation in linked steps of cargo transport along the recycling pathway (de Renzis et al., 2002; Sonnichsen et al., 2000), which may also explain the localization pattern of Bchs and Rab11.

BEACH proteins and membrane traffic

In addition to Bchs, other BEACH family proteins, such as Lyst and Neurobeachin, have been implicated in vesicle trafficking. Mutations in *Lyst* result in the accumulation of giant lysosomes in the cells of both *beige* mutant mice and Chédiak-Higashi syndrome patients, suggesting that Lyst is involved in lysosome trafficking, fusion or formation (Introne et al., 1999). Mouse Neurobeachin mutants lack evoked synaptic transmission at the NMJ, implicating neurobeachin in neurotransmitter release (Su et al., 2004). Our finding that Bchs antagonizes Rab11 raises the intriguing possibility that other BEACH proteins might also interact with Rab family members. It will be interesting to determine whether the defects observed in *Lyst* and neurobeachin mutants reflect the altered activity of particular Rabs and whether alterations in Rab function could ameliorate defects caused by the absence of Lyst or Neurobeachin.

We thank I. Rebay, R. Cohen, M. Gonzalez-Gaitan, D. Ready, H. Bellen, T. Littleton and the Bloomington Stock Center for flies and reagents; B. Adolfsen and T. Littleton for sucrose gradient fractions; T. Mosca and J. Salogiannis for training and assistance; and the DDRC Imaging Core of Children's Hospital. This work was supported by grants from the NEI (EY013874, P.A.G.) and NINDS (NS041062, T.L.S). R.K. was supported by the Medical Scientist Training Program 5T32GM007753-28.

References

Adolfsen, B., Saraswati, S., Yoshihara, M. and Littleton, J. T. (2004). Synaptotagmins are trafficked to distinct subcellular domains including the postsynaptic compartment. *J. Cell Biol.* **166**, 249-260.

Beronja, S., Laprise, P., Papoulas, O., Pellikka, M., Sisson, J. and Tepass, U. (2005). Essential function of Drosophila Sec6 in apical exocytosis of epithelial photoreceptor cells. *J. Cell Biol.* **169**, 635-646.

Brand, A. H. and Perrimon, N. (1993). Targeted gene expression as a means of altering cell fates and generating dominant phenotypes. *Development* **118**, 401-415.

Castermans, D., Wilquet, V., Parthoens, E., Huysmans, C., Steyaert, J., Swinnen, L., Fryns, J. P., Van de Ven, W. and Devriendt, K. (2003). The neurobeachin gene is disrupted by a translocation in a patient with idiopathic autism. *J. Med. Genet.* **40**, 352-356.

Chang, H. C., Newmyer, S. L., Hull, M. J., Ebersold, M., Schmid, S. L. and Mellman, I. (2002). Hsc70 is required for endocytosis and clathrin function in Drosophila. *J. Cell Biol.* **159**, 477-487.

Chen, W., Feng, Y., Chen, D. and Wandinger-Ness, A. (1998). Rab11 is required for trans-golgi network-to-plasma membrane transport and a preferential target for GDP dissociation inhibitor. *Mol. Biol. Cell* **9**, 3241-3257.

Coyle, I. P., Koh, Y. H., Lee, W. C., Slind, J., Fergestad, T., Littleton, J. T. and Ganetzky, B. (2004). Nervous wreck, an SH3 adaptor protein that interacts with Wsp, regulates synaptic growth in Drosophila. *Neuron* **41**, 521-534.

De Lozanne, A. (2003). The role of BEACH proteins in Dictyostelium. *Traffic* **4**, 6-12.

de Renzis, S., Sonnichsen, B. and Zerial, M. (2002). Divalent Rab effectors regulate the sub-compartmental organization and sorting of early endosomes. *Nat. Cell Biol.* **4**, 124-133.

DiAntonio, A., Burgess, R. W., Chin, A. C., Deitcher, D. L., Scheller, R. H. and Schwarz, T. L. (1993). Identification and characterization of Drosophila genes for synaptic vesicle proteins. *J. Neurosci.* **13**, 4924-4935.

Dickman, D. K., Lu, Z., Meinertzhagen, I. A. and Schwarz, T. L. (2006). Altered synaptic development and active zone spacing in endocytosis mutants. *Curr. Biol.* **16**, 591-598.

Dollar, G., Struckhoff, E., Michaud, J. and Cohen, R. S. (2002). Rab11 polarization of the Drosophila oocyte: a novel link between membrane trafficking, microtubule organization, and oskar mRNA localization and translation. *Development* **129**, 517-526.

Finley, K. D., Edeen, P. T., Cumming, R. C., Mardahl-Dumesnil, M. D., Taylor, B. J., Rodriguez, M. H., Hwang, C. E., Benedetti, M. and McKeown, M. (2003). blue cheese mutations define a novel, conserved gene involved in progressive neural degeneration. *J. Neurosci.* **23**, 1254-1264.

Fujita, S. C., Zipursky, S. L., Benzer, S., Ferrus, A. and Shotwell, S. L. (1982).

Monoclonal antibodies against the Drosophila nervous system. *Proc. Natl. Acad. Sci. USA* **79**, 7929-7933.
Garrity, P. A., Lee, C. H., Salecker, I., Robertson, H. C., Desai, C. J., Zinn, K. and Zipursky, S. L. (1999). Retinal axon target selection in Drosophila is regulated by a receptor protein tyrosine phosphatase. *Neuron* **22**, 707-717.
Hanesch, U., Fischbach, K. F. and Heisenberg, M. (1989). Neuronal architecture of the central complex in *Drosophila melanogaster*. *Cell Tissue Res.* **257**, 343-366.
Harris, E., Wang, N., Wu, W.-I., Weatherford, A., De Lozanne, A. and Cardelli, J. (2002). Dictyostelium LvsB mutants model the lysosomal defects associated with Chediak-Higashi syndrome. *Mol. Biol. Cell* **13**, 656-669.
Harrison, S. D., Broadie, K., van de Goor, J. and Rubin, G. M. (1994). Mutations in the Drosophila Rop gene suggest a function in general secretion and synaptic transmission. *Neuron* **13**, 555-566.
Introne, W., Boissy, R. E. and Gahl, W. A. (1999). Clinical, molecular, and cell biological aspects of Chediak-Higashi syndrome. *Mol. Genet. Metab.* **68**, 283-303.
Jafar-Nejad, H., Andrews, H. K., Acar, M., Bayat, V., Wirtz-Peitz, F., Mehta, S. Q., Knoblich, J. A. and Bellen, H. J. (2005). Sec15, a component of the exocyst, promotes notch signaling during the asymmetric division of Drosophila sensory organ precursors. *Dev. Cell* **9**, 351-363.
Jankovics, F., Sinka, R. and Erdelyi, M. (2001). An interaction type of genetic screen reveals a role of the Rab11 gene in oskar mRNA localization in the developing Drosophila melanogaster oocyte. *Genetics* **158**, 1177-1188.
Jogl, G., Shen, Y., Gebauer, D., Li, J., Wiegmann, K., Kashkar, H., Kronke, M. and Tong, L. (2002). Crystal structure of the BEACH domain reveals an unusual fold and extensive association with a novel PH domain. *EMBO J.* **21**, 4785-4795.
Kraut, R., Menon, K. and Zinn, K. (2001). A gain-of-function screen for genes controlling motor axon guidance and synaptogenesis in Drosophila. *Curr. Biol.* **11**, 417-430.
Kwak, E., Gerald, N., Larochelle, D. A., Vithalani, K. K., Niswonger, M. L., Maready, M. and De Lozanne, A. (1999). LvsA, a protein related to the mouse beige protein, is required for cytokinesis in Dictyostelium. *Mol. Biol. Cell* **10**, 4429-4439.
Lewis, E. B. and Bacher, F. (1968). Mutagenesis with ethyl methanesulfonate. *Drosoph. Inf. Serv.* **43**, 193.
Littleton, J. T., Bellen, H. J. and Perin, M. S. (1993). Expression of synaptotagmin in Drosophila reveals transport and localization of synaptic vesicles to the synapse. *Development* **118**, 1077-1088.
Marie, B., Sweeney, S. T., Poskanzer, K. E., Roos, J., Kelly, R. B. and Davis, G. W. (2004). Dap160/intersectin scaffolds the periactive zone to achieve high-fidelity endocytosis and normal synaptic growth. *Neuron* **43**, 207-219.
Misra, S., Miller, G. J. and Hurley, J. H. (2001). Recognizing phosphatidylinositol 3-phosphate. *Cell* **107**, 559-562.
Murthy, M., Garza, D., Scheller, R. H. and Schwarz, T. L. (2003). Mutations in the exocyst component Sec5 disrupt neuronal membrane traffic, but neurotransmitter release persists. *Neuron* **37**, 433-447.
Nagle, D. L., Karim, M. A., Woolf, E. A., Holmgren, L., Bork, P., Misumi, D. J., McGrail, S. H., Dussault, B. J., Jr, Perou, C. M., Boissy, R. E. et al. (1996). Identification and mutation analysis of the complete gene for Chediak-Higashi syndrome. *Nat. Genet.* **14**, 307-311.
Pelissier, A., Chauvin, J. P. and Lecuit, T. (2003). Trafficking through Rab11 endosomes is required for cellularization during Drosophila embryogenesis. *Curr. Biol.* **13**, 1848-1857.
Pfeffer, S. and Aivazian, D. (2004). Targeting Rab GTPases to distinct membrane compartments. *Nat. Rev. Mol. Cell Biol.* **5**, 886-896.
Rao, S., Lang, C., Levitan, E. S. and Deitcher, D. L. (2001). Visualization of neuropeptide expression, transport, and exocytosis in Drosophila melanogaster. *J. Neurobiol.* **49**, 159-172.
Ren, M., Xu, G., Zeng, J., De Lemos-Chiarandini, C., Adesnik, M. and Sabatini, D. D. (1998). Hydrolysis of GTP on rab11 is required for the direct delivery of transferrin from the pericentriolar recycling compartment to the cell surface but not from sorting endosomes. *Proc. Natl. Acad. Sci. USA* **95**, 6187-6192.
Riggs, B., Rothwell, W., Mische, S., Hickson, G. R., Matheson, J., Hays, T. S., Gould, G. W. and Sullivan, W. (2003). Actin cytoskeleton remodeling during early Drosophila furrow formation requires recycling endosomal components Nuclear-fallout and Rab11. *J. Cell Biol.* **163**, 143-154.
Rorth, P. (1996). A modular misexpression screen in Drosophila detecting tissue-specific phenotypes. *Proc. Natl. Acad. Sci. USA* **93**, 12418-12422.
Satoh, A. K., O'Tousa, J. E., Ozaki, K. and Ready, D. F. (2005). Rab11 mediates post-Golgi trafficking of rhodopsin to the photosensitive apical membrane of Drosophila photoreceptors. *Development* **132**, 1487-1497.
Schulze, K. L., Broadie, K., Perin, M. S. and Bellen, H. J. (1995). Genetic and electrophysiological studies of Drosophila syntaxin-1A demonstrate its role in nonneuronal secretion and neurotransmission. *Cell* **80**, 311-320.
Schuster, C. M., Davis, G. W., Fetter, R. D. and Goodman, C. S. (1996). Genetic dissection of structural and functional components of synaptic plasticity. II. Fasciclin II controls presynaptic structural plasticity. *Neuron* **17**, 655-667.
Seabra, M. C. and Wasmeier, C. (2004). Controlling the location and activation of Rab GTPases. *Curr. Opin. Cell Biol.* **16**, 451-457.
Sonnichsen, B., De Renzis, S., Nielsen, E., Rietdorf, J. and Zerial, M. (2000). Distinct membrane domains on endosomes in the recycling pathway visualized by multicolor imaging of Rab4, Rab5, and Rab11. *J. Cell Biol.* **149**, 901-914.
Su, Y., Balice-Gordon, R. J., Hess, D. M., Landsman, D. S., Minarcik, J., Golden, J., Hurwitz, I., Liebhaber, S. A. and Cooke, N. E. (2004). Neurobeachin is essential for neuromuscular synaptic transmission. *J. Neurosci.* **24**, 3627-3636.
Sweeney, S. T. and Davis, G. W. (2002). Unrestricted synaptic growth in spinster-a late endosomal protein implicated in TGF-beta-mediated synaptic growth regulation. *Neuron* **36**, 403-416.
Tautz, D. and Pfeifle, C. (1989). A non-radioactive in situ hybridization method for the localization of specific RNAs in Drosophila embryos reveals translational control of the segmentation gene hunchback. *Chromosoma* **98**, 81-85.
Ullrich, O., Reinsch, S., Urbe, S., Zerial, M. and Parton, R. G. (1996). Rab11 regulates recycling through the pericentriolar recycling endosome. *J. Cell Biol.* **135**, 913-924.
Wang, J., Zugates, C. T., Liang, I. H., Lee, C. H. and Lee, T. (2002). Drosophila Dscam is required for divergent segregation of sister branches and suppresses ectopic bifurcation of axons. *Neuron* **33**, 559-571.
Wang, J. W., Gamsby, J. J., Highfill, S. L., Mora, L. B., Bloom, G. C., Yeatman, T. J., Pan, T. C., Ramne, A. L., Chodosh, L. A., Cress, W. D. et al. (2004). Deregulated expression of LRBA facilitates cancer cell growth. *Oncogene* **23**, 4089-4097.
Wang, N., Wu, W.-I. and De Lozanne, A. (2002). BEACH family of proteins: phylogenetic and functional analysis of six Dictyostelium BEACH proteins. *J. Cell. Biochem.* **86**, 561-570.
Ward, E. S., Martinez, C., Vaccaro, C., Zhou, J., Tang, Q. and Ober, R. J. (2005). From sorting endosomes to exocytosis: association of Rab4 and Rab11 GTPases with the Fc receptor, FcRn, during recycling. *Mol. Biol. Cell* **16**, 2028-2038.
Wucherpfennig, T., Wilsch-Brauninger, M. and Gonzalez-Gaitan, M. (2003). Role of Drosophila Rab5 during endosomal trafficking at the synapse and evoked neurotransmitter release. *J. Cell Biol.* **161**, 609-624.
Zerial, M. and McBride, H. (2001). Rab proteins as membrane organizers. *Nat. Rev. Mol. Cell Biol.* **2**, 107-117.
Zhang, X. M., Ellis, S., Sriratana, A., Mitchell, C. A. and Rowe, T. (2004). Sec15 is an effector for the Rab11 GTPase in mammalian cells. *J. Biol. Chem.* **279**, 43027-43034.